

Initial Steps of Rubicene Film Growth on Silicon Dioxide

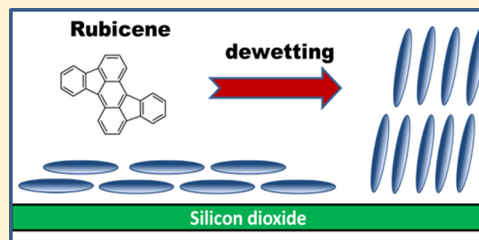
Boris Scherwitzl,[†] Walter Lukesch,[†] Andreas Hirzer,[†] Jörg Albering,[‡] Günther Leising,[†] Roland Resel,[†] and Adolf Winkler^{*,†}

[†]Institute of Solid State Physics, Graz University of Technology, Petersgasse 16, A-8010 Graz, Austria

[‡]Graz University of Technology, Mandellstrasse 11, 8010 Graz, Austria

 Supporting Information

ABSTRACT: The film growth of the conjugated organic molecule rubicene on silicon dioxide was studied in detail. Since no structural data of the condensed material were available, we first produced high quality single crystals from solution and determined the crystal structure. This high purity material was used to prepare ultrathin films under ultrahigh vacuum conditions, by physical vapor deposition. Thermal desorption spectroscopy (TDS) was applied to delineate the adsorption and desorption kinetics. It could be shown that the initial sticking coefficient is only 0.2 ± 0.05 , but the sticking coefficient increases with increasing coverage. TDS further revealed that first a closed, weakly bound bilayer develops (wetting layer), which dewets after further deposition of rubicene, leading to an island-like layer. These islands are crystalline and exhibit the same structure as the solution grown crystals. The orientation of the crystallites is with the (001) plane parallel to the substrate. A dewetting of the closed bilayer was also observed when the film was exposed to air. Furthermore, Ostwald ripening of the island-like film takes place under ambient conditions, leading to films composed of few, large crystallites. From TDS, we determined the heat of evaporation from the multilayer islands to be 1.47 eV, whereas the desorption energy from the first layer is only 1.25 eV.



1. INTRODUCTION

Organic thin films have attracted high and widespread scientific interest within the past decade. In particular, films composed of conjugated materials, polymers, as well as molecules are of preferred importance. This is due to their interesting and advantageous electrical,¹ optical,² optoelectronic,³ chemical, and mechanical properties, which makes such films attractive for applications in organic electronics and optoelectronics. One of the powerful aspects of conjugated systems is the adjustability of the electronic structure, especially the band gap, based on the individual extent of the π -conjugation within the main chain (in the case of polymers) or within the single molecule (in the case of conjugated oligomers or conjugated molecules). Moreover, the electronic structure of the bulk of conjugated systems (single crystals, thin films) can be strongly tuned by the crystallographic packing of single molecules with respect to each other.⁴ This tuning possibility makes them attractive for many optical, electronic, and optoelectronic applications. Other advantageous aspects of organic films are their softness, which allows the production of flexible electronics, the expected low production costs, and a possibly better environmental compatibility. On the other hand, there are also some drawbacks in the endeavor to produce and maintain high quality organic films: poor air stability, deterioration with time, dewetting, and in particular difficulties to produce highly defined layer-like films.

In this article, we focus on the initial steps of film formation of rubicene molecules. Rubicene ($C_{26}H_{14}$) is a polycyclic hydrocarbon consisting of five benzene rings with three linearly

fused rings and one benzene ring at each diagonal side, shown in Figure 1 and in the inset of Figure 2a. It is a stiff and planar semiconducting molecule with a molecular weight of $m = 326.4$ amu, a density of $\rho = 1.392$ g/cm³, and a melting point of $T_m = 581$ K. Interestingly, this material is poorly investigated; so far

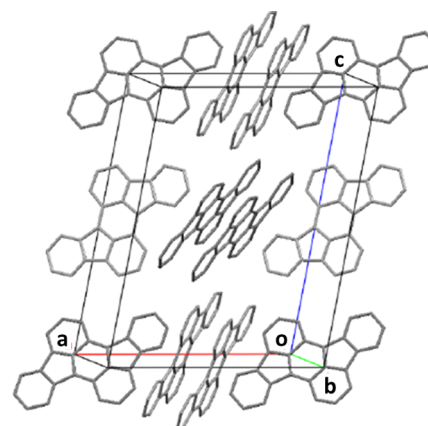


Figure 1. Package of the molecules in the rubicene crystal, together with the crystal unit cell. The Bravais lattice is primitive monoclinic. The basis consists of four molecules, arranged in a parallel stacking structure.

Received: December 13, 2012

Revised: January 29, 2013

Published: January 31, 2013

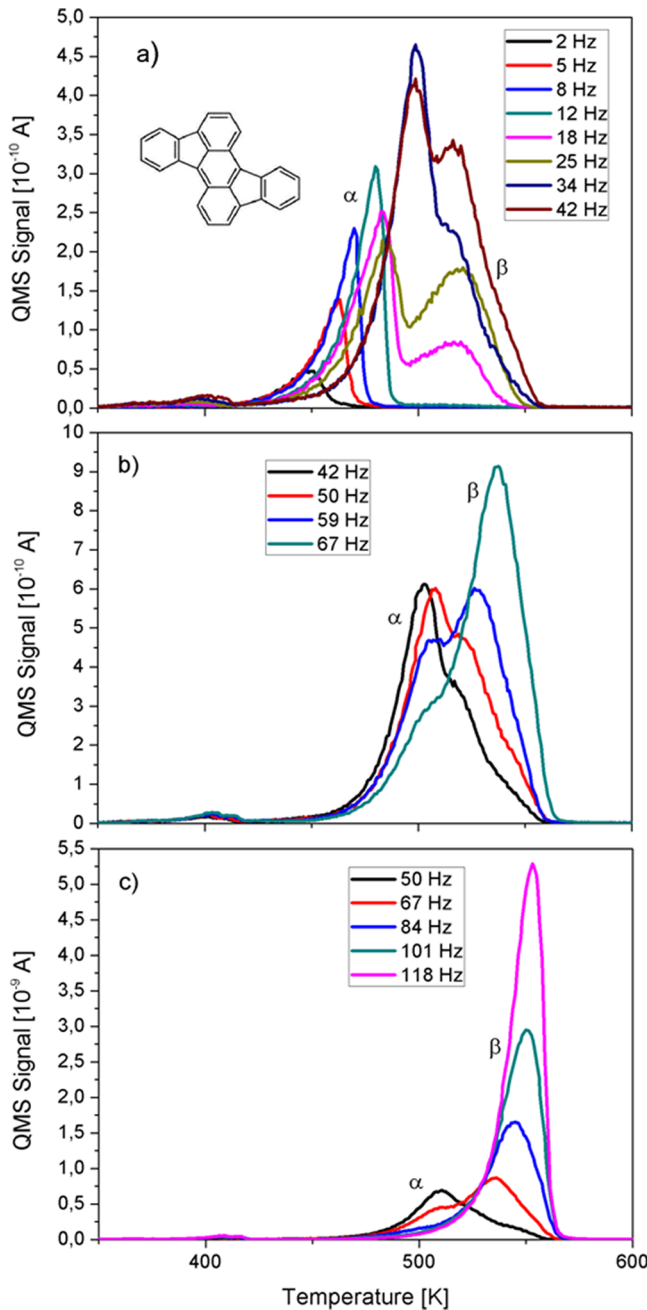


Figure 2. Thermal desorption spectra of rubicene from carbon covered silicon dioxide, for different exposures. Adsorption temperature $T_{ad} = 220$ K, heating rate $\beta = 1$ K/s. The exposure is given in Hz, as determined by a quartz microbalance: (a) 2–42 Hz, (b) 42–67 Hz, (c) 50–118 Hz. The chemical structure of rubicene is shown in the inset of part a.

nothing is known about the crystallography of condensed rubicene and the formation of rubicene thin films. One important aspect is that rubicene films can be produced both from solution and by thermal evaporation under vacuum conditions. In this work, we first prepared rubicene single crystals from solution for their structural identification and then used this high purity material to prepare thin films under ultrahigh vacuum conditions. Under these well controlled conditions, we studied the adsorption and desorption properties of rubicene on silicon dioxide and the initial steps of film formation by using thermal desorption spectroscopy. In

addition, we were able to study the thermal and air stability of ultrathin rubicene films. Atomic force microscopy revealed that the rubicene films are composed of randomly oriented islands. Dewetting and islanding is a pronounced feature of this material.

2. EXPERIMENTAL SECTION

2.1. Rubicene Purification, Crystal Growth, and Characterization. The rubicene powder, as purchased from Arcos Organics, Belgium, has a purity of 98%. To provide a high chemical purity of the grown crystals, as well as for the thin films, the purchased rubicene material was thoroughly purified by a gas transport technique. The purity was verified by optical spectroscopy (absorption and luminescence excitation and emission) of highly concentrated solutions, as well as by infrared absorption spectroscopy in the spectral range of the C–H stretching vibrations (2800 – 3100 cm $^{-1}$) (see the Supporting Information, Figures SI-1, SI-2, and SI-3).

Rubicene single crystals were grown from a rubicene–toluene solution which resulted in elongated crystals of several mm lengths. The XRD measurements were carried out on a Bruker Kappa APEX II 4K CCD diffractometer using graphite monochromated Mo $K\alpha$ radiation with a characteristic wavelength of 0.71 Å. Moreover, it can envelope the specimen in a cold nitrogen gas stream to permit crystallographic studies at low temperatures to improve the accuracy of the structural data. The crystal structure of rubicene was determined at 100 and 250 K. All calculations were performed using the Bruker APEX II program system⁵ and the SHELXTL program package.⁶ Absorption corrections were performed by the program SADABS⁷ (see the Supporting Information).

2.2. Thin Film Deposition. Ultrathin rubicene films were prepared under ultrahigh vacuum conditions by physical vapor deposition from a Knudsen cell. The substrates were silicon dioxides (thickness 150 nm) thermally grown on 0.67 mm thick Si(100) wafers (10 mm \times 10 mm), as supplied by Siegert Consulting e.K., Germany. A quartz microbalance thin film monitor (Inficon XTM/2) was used to quantitatively determine the evaporation rate from the Knudsen cell and hence the deposited amount of rubicene on the SiO_2/Si substrate. For this purpose, the sample was temporarily replaced by the microbalance. Typically, deposition rates of 70 ng/(min·cm 2), equivalent to 0.5 nm/min, were applied, which required a Knudsen cell temperature of about 470 K. The sample temperature during deposition was either room temperature or 220 K, as obtained by LN_2 cooling. The residual pressure during deposition was in the 10^{-9} mbar range.

2.3. Substrate and Thin Film Characterization. The chemical compositions of the substrate and thin films were analyzed by Auger electron spectroscopy (AES) (Varian CMA). On the freshly installed sample, in addition to silicon and oxygen, carbon was observed as a contaminant. This carbon could be easily removed by 10 min of argon sputtering (500 V, 30 mA, 5×10^{-5} mbar argon), resulting in a clean substrate. However, annealing to 800 K again resulted in some accumulation of carbon, most probably due to segregation from the bulk. As we will show below, this carbon contamination on the silicon dioxide surface had no significant influence on the adsorption behavior of rubicene. The Auger analysis of the deposited rubicene film exhibited just carbon; no impurities could be seen. However, one has to be careful by interpreting the carbon signal in this case, because there is strong evidence that rubicene dissociates in the area where the

electron beam hits the surface. The morphology of the prepared films was determined *ex situ* by atomic force microscopy (AFM) in the tapping mode (Nanosurf Easyscan2). The crystallographic structure of the ultrathin films was investigated by X-ray diffraction. A Philips X'Pert System equipped with an ATC3 cradle was used in Bragg–Brentano focusing geometry. Radiation of a sealed chromium tube was used in combination with a graphite monochromator at the secondary side.

2.4. Thermal Desorption Spectroscopy. A quite powerful method to determine the thermal stability and the quantitative amount of deposited rubicene is thermal desorption spectroscopy (TDS). In this case, the rubicene covered sample is heated up to 800 K, typically with heating rates of 1 K/s, and the desorbing molecules are detected with a mass spectrometer. The integral over the spectrum is a measure for the deposited amount. From the shape of the spectra and the peak maxima, conclusions can be drawn regarding the desorption order and the desorption energy. Furthermore, from a series of desorption spectra with different adsorbed amounts, one can get information on the adsorption kinetics, the layer formation, and the desorption kinetics.⁸ For TDS, we have tuned the mass spectrometer (Balzers Quadstar) to mass 163, because this showed the highest number of fragments in the cracking pattern. In order to perform TDS on a silicon wafer, the samples were attached to a stainless steel plate via tantalum clamps, as described in more detail elsewhere.⁹ In this context, we have to express a caveat with respect to the desorption temperature. Due to the poor heat conductivity of SiO₂ and the thermal contact resistance between the (oxidized) silicon wafer and the steel plate, the temperature of the sample surface lags behind the temperature of the heating plate. Although one can take this into account by a simple first-order correction⁹ (see the Supporting Information), in the following, we will use the uncorrected temperature values, if not stated otherwise.

3. EXPERIMENTAL RESULTS

3.1. Crystal Structure. So far, no structural characterization for rubicene single crystals existed in the literature. Our X-ray diffraction measurements revealed that the crystal system of rubicene is monoclinic and its Bravais lattice is primitive monoclinic (space group $P2_1/n$). Figure 1 depicts the package of the molecules in the rubicene crystal. The XRD measurements yield the following unit cell dimensions at $T = 250$ K: $a = 16.158(1)$ Å, $b = 5.1230(4)$ Å, $c = 19.112(1)$ Å, $\beta = 97.22^\circ$. With these dimension values, one gets $V = 1569.5(2)$ Å³. Since the unit cell basis contains four molecules, the rubicene crystal density is calculated to be $\rho = 1.381$ g/cm³. This is in good agreement with the literature data.¹⁰ Furthermore, the interplanar distance between two adjacent parallel molecules in the rubicene crystal is 3.38 Å. The observed molecular packing is typical for aromatic molecules with dislike shape.¹¹ All grown crystals were also analyzed at a temperature of 100 K. Since the structural results were almost identical for both temperatures, neither a phase transition nor a significant change in the crystal structure occurs in the temperature range between 100 and 250 K (see the Supporting Information). The crystallographic data for the structures have also been deposited with the Cambridge Crystallographic Data Centre.¹²

3.2. Thermal Desorption Spectra. As outlined above, thermal desorption spectroscopy can be applied to delineate the kinetics of adsorption and desorption of particles on and from substrates. Albeit this method has been mainly applied in

classical surface science to study reactions at surfaces, it has proven to also be very powerful to describe the initial stages of organic film growth.¹³ In Figure 2, desorption spectra of rubicene from silicon dioxide after different exposed amounts at 220 K are depicted. In this particular case, the substrate surface was covered with some carbon. Actually, after each deposition of rubicene and subsequent heating to 800 K, a specific amount of carbon remains on the surface. This amount accumulates to a saturation value above which no further decomposition of rubicene can be observed (Auger ratio C272/O510 ≈ 0.27). Therefore, we used this stable substrate for the adsorption/desorption experiments. For better visibility, the spectra are plotted in three different figures for different coverage regimes.

The exposed amounts of rubicene are described by the frequency changes of a quartz microbalance, which was positioned at the place of the substrate before the actual deposition at the substrate, in order to install a specific deposition rate. From the known quartz frequency ($f \approx 6$ MHz), the quartz sensitivity ($S = 2.26 \times 10^{-6}$ cm²s/g), and the density of rubicene ($\rho = 1.39$ g/cm³), one can determine the correlation between the quartz frequency change (Δf) and the mean thickness (d) of the exposed amount. According to the relationship¹⁴

$$d = -S^{-1} \Delta f / (f^2 \rho) \quad (1)$$

it follows that a frequency change of 1 Hz equals a mean thickness change of 0.9 Å exposed rubicene. It should be emphasized at this point that the deposited amount equals the exposed amount only if the sticking coefficient is 1. We will show below that this is not the case for rubicene on silicon dioxide in the low coverage regime.

In Figure 2a, a series of spectra for exposures between 2 and 42 Hz are compiled. For very low exposure (2–12 Hz), only a single peak is observed, designated as the α -peak, which shifts to higher temperatures with increasing adsorbed amount. Above 12 Hz, this peak increases further and shifts to even higher temperatures, but a second peak at approximately 30 K higher temperature, designated as the β -peak, appears at the same time. With further coverage increase (Figure 2b), the α -peak starts to decrease, while the β -peak still increases (42–67 Hz). Finally, with even further coverage increase (50–118 Hz), the α -peak totally disappears and the β -peak continues to increase with a common leading edge (Figure 2c).

3.3. Sticking Coefficient. In order to interpret the specific behavior of the desorption spectra, we have to determine the actual amount of adsorbed/desorbed material. For this purpose, we have plotted the areas of the individual desorption spectra, which are proportional to the adsorbed/desorbed amount, versus the exposed amount as measured by the quartz microbalance (Figure 3). The most remarkable result of this presentation is the increasing slope with increasing adsorbed amount. This means that the sticking coefficient for rubicene increases with increasing coverage. Usually, it is assumed that the initial sticking coefficient of organic molecules at and below room temperature is 1.^{15,16} Apparently, this is not the case for the adsorption of rubicene on silicon dioxide. If we assume that the maximum slope (α_2) in Figure 3 is close to 1, the initial slope (α_1) is about 0.25. Considering this sticking coefficient, we can convert the exposure values, given in Hz, into values for the adsorbed amount, described by the mean thickness (Å).

3.4. Influence of Surface Cleanliness. In order to check the influence of surface cleanliness on the adsorption behavior, we have performed adsorption/desorption experiments on a

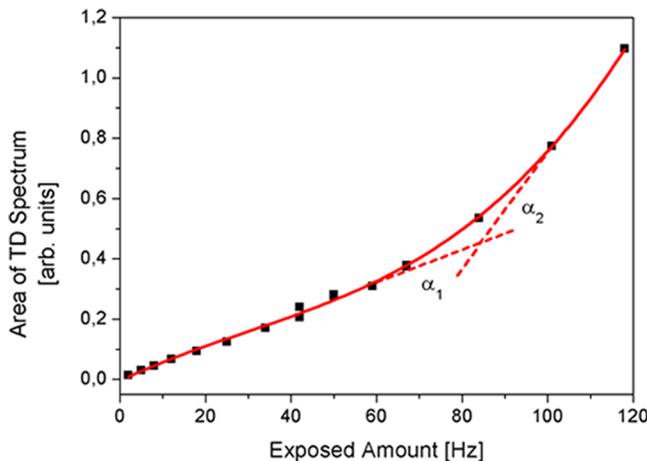


Figure 3. TDS area for rubicene desorbed from carbon covered silicon dioxide as a function of the exposed amount, as measured by the quartz microbalance. Adsorption temperature: 220 K.

silicon dioxide surface which was cleaned by argon sputtering before each rubicene deposition. A set of thermal desorption spectra is shown in the Supporting Information (Figure SI-7). The result is similar to that on the carbon contaminated substrate. First, a single peak (α) at low temperature appears until at about 14 Hz a second peak (β) at higher temperatures starts to grow. The α -peak grows further to about double intensity, before it starts to decrease and finally disappears completely, whereas the β -peak continues to grow with exposure. The corresponding relationship between exposure and adsorbed amount is depicted in Figure SI-8 of the Supporting Information. Again, the slope of the coverage curve increases with increasing coverage. Assuming a slope of 1 in the high coverage regime yields an initial slope (initial sticking coefficient) of about 0.17. This is within the experimental error similar to that on the carbon covered substrate.

3.5. Heat of Evaporation. The desorption spectra for high rubicene coverage (Figure 2c) show close to zero-order desorption kinetics. From such spectra, one can deduce the desorption energy, equivalent to the heat of evaporation. Unfortunately, as outlined above, the exact temperature of the substrate surface is not known, due to poor heat conductivity between the oxidized silicon wafer and the stainless steel heating plate. In order to obtain a reliable value for the heat of evaporation, we have adsorbed/desorbed rubicene directly on/from the steel plate sample holder, where the temperature is measured with the thermocouple. A corresponding desorption spectrum for an exposure of 100 Hz shows a peak maximum at about 390 K (see the Supporting Information, Figure SI-10). A comparison with Figure 2 clearly shows the temperature lag of desorption from the silicon dioxide surface. However, one can observe in those spectra a small peak at around 400 K, which stems from desorption from the tantalum foils, which are used to clamp the silicon wafer to the steel plate sample holder. Thus, a first-order temperature correction can be applied which allows the determination of the desorption energy for monolayer and multilayer desorption (see the Supporting Information).

The desorption rate R_{des} for zero-order (multilayer) desorption and first-order (monolayer) desorption can be described by the Polanyi–Wigner equation:¹⁷

$$R_{\text{des}} = \nu \cdot \Theta^n \cdot N_{\text{ML}} \exp\left(-\frac{E_{\text{des}}}{kT}\right) \quad (2)$$

with ν being the frequency factor, Θ the coverage, n the desorption order, and N_{ML} the number of molecules in the monolayer. Hence, plotting the logarithm of the desorption rate R_{des} (QMS signal) versus $1/T$ should yield a straight line with a slope equivalent to (E_{des}/k) . For multilayer desorption, where the molecule density in the (001) plane of rubicene is 2.4×10^{14} molecules/cm², the calculation yields a desorption energy of 1.47 ± 0.05 eV. Furthermore, from the intercept with the Y-axis, we obtain a frequency factor of $\nu = 3 \times 10^{18}$ s⁻¹. We have also performed independent measurements of the heat of evaporation by determining the evaporation rate from our Knudsen cell, measured by the microbalance, as a function of the cell temperature. The evaluation of these data yields a heat of evaporation of 1.49 ± 0.05 eV, in good agreement with the multilayer desorption energy (see the Supporting Information, Figure SI-9).

By using the same temperature correction, one can also evaluate the desorption spectra in the monolayer regime, by assuming first-order desorption. In this case, $\ln(R_{\text{des}}/\Theta)$ has to be plotted versus $1/T$. With a molecule density of 8.9×10^{13} molecules/cm² for a dense packed monolayer of lying molecules, the evaluation of the 12 Hz spectrum in Figure 2a yields $E_{\text{des}} = 1.25$ eV and $\nu = 3 \times 10^{16}$ s⁻¹ (see the Supporting Information, Figures SI-11 and SI-12).

3.6. Film Morphology and Dewetting. Thermal desorption spectroscopy has suggested that rubicene first forms two layers of flat-lying molecules. With increasing deposition, however, these layers dewet and the molecules form islands. This could be proven by ex situ atomic force microscopy. In Figure 4, an AFM image of a rubicene film after an exposure of 250 Hz is shown, equivalent to a mean layer thickness of about 20 nm, considering the reduced sticking coefficient at low coverage. The film consists of randomly oriented islands with elongated shape. Interestingly, for very low coverage (e.g., 7 Hz, mean thickness: 0.16 nm), for which TDS reveals a layer-like monolayer film, ex situ AFM shows again an island-like morphology (Figure 5). Actually, an integration over all islands shows that all material is contained in the islands and there is no hint of a remaining wetting layer. This strange behavior can be explained by a dewetting process caused by the exposure of the sample to air. Such a venting induced dewetting has been recently demonstrated for the system hexaphenyl on mica.¹⁸ Indeed, a desorption experiment on a 7 Hz rubicene film once performed directly after deposition and once performed after venting the vacuum chamber and re-evacuation showed a dramatic difference (Figure 6). Whereas in the first case one can see mainly desorption from the weakly adsorbed wetting layer, after venting, only desorption from the more strongly bound islands is observed. In addition, the total area under the desorption spectrum has decreased by about 40% after venting.

However, not only the exposure of the thin rubicene film to air changes the morphology, but there is also a further gradual change of the morphology as a function of the storage time in air. This is shown in the AFM images for a 30 Hz film (mean thickness: 0.7 nm), which were obtained directly after venting the chamber and dismounting (Figure 7) and after 24 h (Figure 8). Furthermore, we could show by AFM that for very thin films the storage of the sample in air results in a continuous

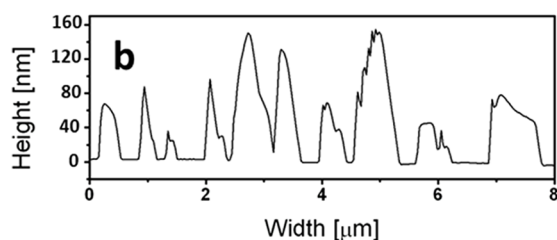
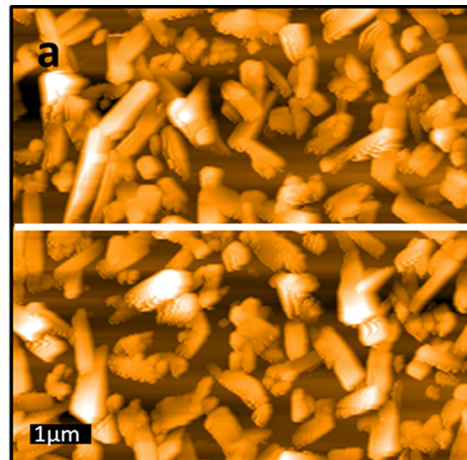


Figure 4. (a) AFM image ($8 \mu\text{m} \times 8 \mu\text{m}$) of a rubicene film on silicon dioxide, with a mean thickness of about 20 nm. Substrate temperature, 300 K; deposition rate, 0.5 nm/min. (b) Cross section along the white line in part a.

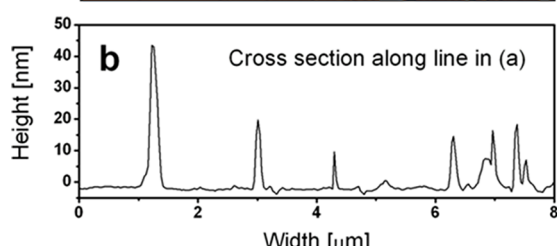
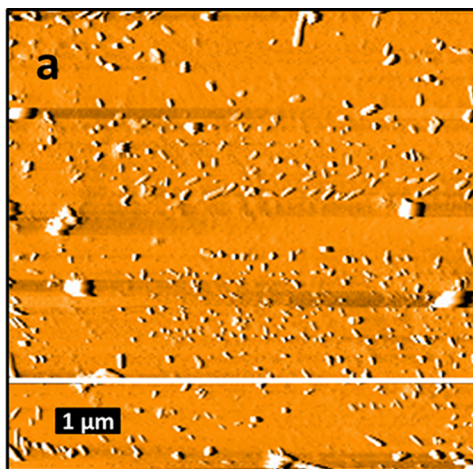


Figure 5. (a) AFM image ($8 \mu\text{m} \times 8 \mu\text{m}$) of a 7 Hz film of rubicene (mean thickness about 0.16 nm) deposited on silicon dioxide at 300 K, immediately measured after dismantling the sample from the vacuum chamber. (b) Cross section along the white line in part a.

decrease of the deposited amount. Particularly, a 7 Hz film was not visible anymore by AFM after storage in air for 5 days.

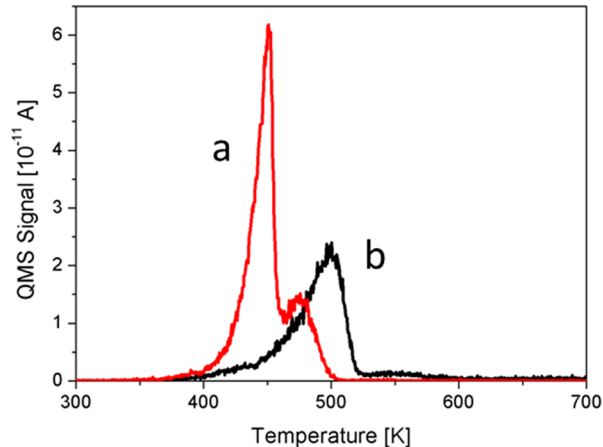


Figure 6. Thermal desorption spectra for a 7 Hz rubicene film obtained directly after deposition (a) and for a film with the same exposure but obtained after venting the vacuum system and re-evacuation (b). Adsorption temperature: 300 K.

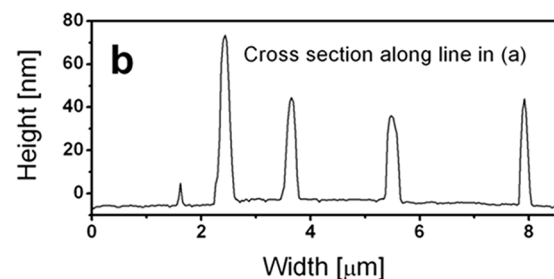
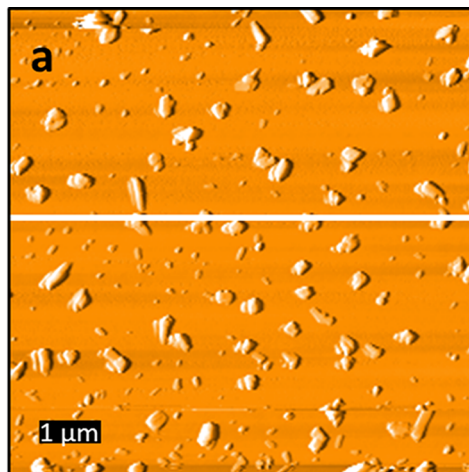


Figure 7. (a) AFM image ($8.6 \mu\text{m} \times 8.6 \mu\text{m}$) of a rubicene film on silicon dioxide, with an initial mean thickness of about 0.7 nm, directly measured after deposition at 300 K and venting the vacuum system. (b) Cross section along the white line in part a.

3.7. X-ray Diffraction on Thin Rubicene Films. The crystallographic structure of a 20 nm thick film (corresponding to Figure 4) was determined by X-ray diffraction. A specular scan ($\Theta/2\Theta$) is shown in Figure 9, revealing that the crystallites are oriented with the (001) plane parallel to the substrate surface. However, from the large rocking width of about 6° , as depicted in the inset of Figure 9, one has to conclude that the mosaicity of the rubicene crystals is large. On the basis of our crystal structure solution together with the observation of the 00L peaks within the specular diffraction, the alignment of the

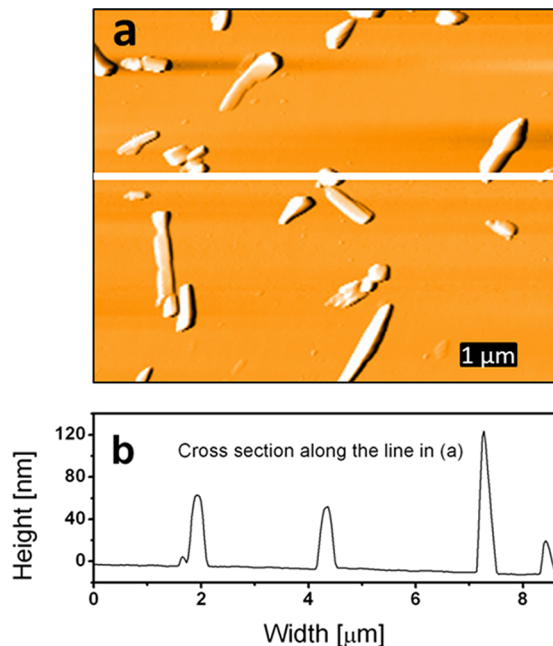


Figure 8. (a) AFM image ($8.6\text{ }\mu\text{m} \times 6.9\text{ }\mu\text{m}$) of a rubicene film deposited on silicon dioxide at 300 K, with an initial mean thickness of about 0.7 nm, measured 24 h after deposition and venting the vacuum system. (b) Cross section along the white line in part a.

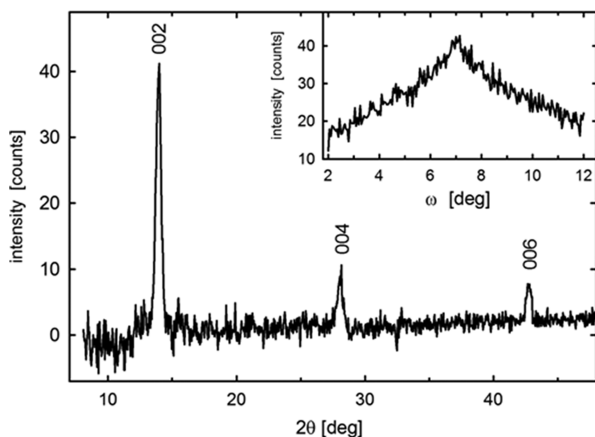


Figure 9. Specular X-ray diffraction scan on a 20 nm thick rubicene film grown on SiO_2 , using $\text{Cr K}\alpha$ radiation. The inset gives the rocking curve of the $00\bar{2}$ peak.

molecules relative to the substrate surface could be determined. The layers of molecules are formed parallel to the substrate surface (Figure 10a). Within one layer, the molecules are stacked parallel to each other so that they form parallel columns; within the columns, the molecules are side-tilted (Figure 10b).

4. DISCUSSION

The initial layer formation of rubicene on silicon dioxide shows a quite peculiar behavior. Typically, on reactive surfaces, small organic molecules form first a strongly bound wetting layer of lying molecules, on which then the multilayer forms, either consisting again of lying molecules or of standing molecules. Examples of the former film formation are quaterphenyl (4P) and hexaphenyl (6P) on $\text{Au}(111)$,^{19,20} 6P on freshly cleaved mica,^{9,21,22} pentacene (5A) on $\text{Au}(111)$,²³ or PTCDA on

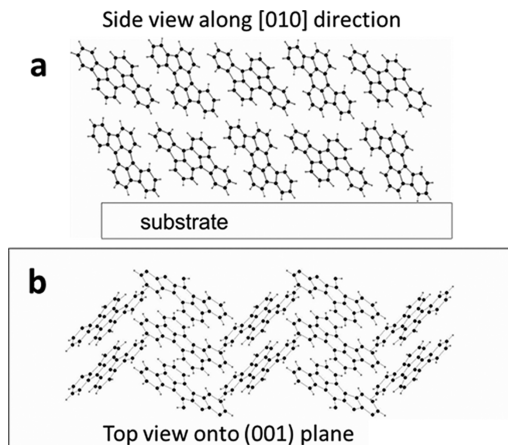


Figure 10. Molecule arrangements in a rubicene crystal. (a) Side view of two molecular layers along the [010] direction. (b) Top view onto the (001) plane of one molecular layer.

$\text{Ag}(111)$,²⁴ to name just a few. An example of the latter layer growth is 5A on $\text{Si}(111)$.²⁵ Contrary, on inert, flat substrates, organic molecules tend to form films consisting of standing molecules, beginning already in the first layer, like for 6P on sputtered mica,⁹ or 5A on SiO_2 .²⁶

Quantitative thermal desorption spectroscopy is, in addition to AFM, a powerful method to distinguish between the monolayer and multilayer formation. Particularly, the energetics and kinetics of film formation and decomposition can be studied with TDS successfully.¹³ Films of the above-mentioned characteristics with a strongly bound wetting layer typically show two desorption peaks, one for multilayer desorption and another one for monolayer desorption at higher temperature. If the first layer already consists of standing molecules, due to weak interaction with the substrate, typically only one desorption peak is observed.¹³

In the case of rubicene desorption at low coverage, first a single peak appears at relatively low temperature. After a particular coverage, this peak starts to decrease and it is finally replaced by a desorption peak at higher temperature. Such a behavior for the first monolayer has not been observed before to the best of our knowledge. There is only one example in the literature where a similar desorption behavior was described, however involving the transition between a second layer and a multilayer. In that case, hexaaza-triphenylene-hexacarbonitrile (HATCN) was adsorbed on $\text{Au}(111)$ ²⁷ and $\text{Ag}(111)$.¹⁶ In both cases, a weakly bound second layer was formed on top of a strongly bound wetting layer, where the second layer was then incorporated at higher coverage into the multilayer by dewetting, from which the molecules desorbed at somewhat higher temperature.

The adsorption/desorption behavior of rubicene on/from silicon dioxide can be explained in the following way: In the submonolayer regime, the molecules adsorb flat-lying on the inert SiO_2 substrate. This interaction is quite weak; the desorption energy is only 1.25 eV. Desorption of this layer appears already slightly above room temperature at around 350 K in the form of a single peak (α -peak). (Note that the temperature scale in Figure 2 is not corrected.) This single peak of asymmetric form shifts to higher temperature with increasing coverage, first with a common leading edge and finally even with the leading edge shifting to higher temperature. This desorption characteristic is an indication of first-order

desorption kinetics with attractive interactions between the molecules.⁸ Desorption proceeds in the form of a single peak up to an exposure of 12–15 Hz. According to the calibration of the quartz microbalance and the experimentally obtained initial sticking coefficient of about 0.25, the saturation of this single peak can be attributed to a coverage of about 0.3 nm mean thickness. This is evidence for a closed monolayer of flat-lying molecules. The van der Waals thickness of aromatic molecules is about 3.5 Å.²⁸

With further exposure, a second desorption peak (β -peak) appears, shifted by about 30 K to higher temperature. At the same time, the α -peak keeps on growing until it reaches saturation at a coverage equivalent to a double layer of lying molecules. The β -peak continually grows with increasing exposure, indicating desorption from a multilayer, while the α -peak decreases until it eventually totally disappears above an exposure of about 80 Hz. This is equivalent to a mean film thickness of 1.8 nm. We can interpret this behavior as follows: After saturation of the first monolayer, further impinging molecules adsorb in the second layer again flat on. However, this double layer is already metastable. Further adsorption on this double layer results in an unstable film and the molecules restructure from a flat-lying double layer to a standing arrangement, which is apparently energetically more favorable. Actually, the formation of a closed double layer before the formation of islands starts on this layer is not so uncommon. A few examples of such a layer growth are PTCDA on Ag(111),²⁴ HATCN on Au(111),²⁷ and sexiphenyl on Cu(110)(2 × 1)O.²⁹

The key point in the rubicene–SiO₂ system is that the binding energy of the molecules to the substrate (1.25 eV) is weaker than the binding energy between rubicene molecules in the bulk phase, which was calculated to be 1.47 eV. However, the diffusion probability of the flat-lying molecules in the submonolayer phase is not high enough to restructure the layer into 3D islands during heating, from where the molecules then would desorb at higher temperature. This latter behavior has been observed for 6P on sputtered mica.¹⁸ Nevertheless, for higher coverage, the tendency of dewetting in the system rubicene–SiO₂ is so high that the growth of smooth, thick films is very unlikely (see Figure 4).

The formation of a full monolayer of flat-lying molecules is only possible during growth in UHV. Exposure of a 7 Hz layer to air again results in a strong dewetting, as shown by AFM (Figure 5). This was also verified by TDS, performed before and after venting with subsequent re-evacuation (Figure 6). While before venting the desorption peak is at around 450 K (uncorrected), indicative of weakly bound molecules to the substrate, the desorption peak has shifted to 500 K after venting, indicative of desorption from 3D islands. Furthermore, the peak area after venting was reduced by about 40%, demonstrating the partial desorption during venting. A venting induced subsequent nucleation has been recently observed for the system 6P-mica.¹⁸ It was assumed that upon venting water adsorbs on the sample surface and diffuses between film and substrate, thus increasing the diffusion probability and/or decreasing the activation energy for nucleation. Such venting induced subsequent nucleation processes are in particular pronounced for very thin films. This should be taken into account whenever AFM images of such films are interpreted.

The quite weak bonding to the substrate (1.25 eV) and the rather low heat of evaporation of 1.47 eV, as obtained from TDS, has further consequences for the deposited rubicene film

on SiO₂ when stored in air. A comparison of the morphology of a 30 Hz film (0.7 nm mean thickness) measured with AFM immediately after exposure to air (Figure 7a) and after 24 h (Figure 8a) shows significant differences. The film is composed of many small islands immediately after venting, with the largest islands having dimensions of about 300 nm in diameter and heights of about 50 nm (Figure 7b). After storage in air for 24 h, only few, large rectangular shaped islands are visible, with heights up to 120 nm (Figure 8b). This phenomenon is known as Ostwald ripening.³⁰ It is again an indication of the weak bonding of the rubicene molecules at the rims of the 3D islands, leading to a quite dense 2D gas phase of rubicene monomers and hence to the growth of large islands at the expense of the small islands, according to the Gibbs–Thompson relation.³⁰ The process of Ostwald ripening and the partial evaporation of the film are relatively more pronounced on very thin films. A clear reduction of the island size after 30 days in air has been observed for the 0.7 nm thick film. Actually, on the 7 Hz film (mean thickness 0.16 nm, Figure 5), no rubicene material whatsoever could be detected on the silicon dioxide after several days in air. Similar morphological changes of organic layers under ambient conditions have recently been observed also for naphthyl end-capped thiophenes deposited on mica.³¹

The morphology of thick films (20 nm mean thickness, Figure 4) shows the existence of randomly oriented crystallites. With X-ray diffraction, we could identify that the structure of the small crystallites is identical to the bulk structure and that the crystallites are oriented with the (001) plane parallel to the substrate (Figure 9). The arrangement of the rubicene molecules within the bulk crystal in two different views is shown in Figure 10. Rocking curve measurements (inset in Figure 9) on this film revealed a quite high fwhm of about 6°, indicating that the mosaicity of the film is rather large, significantly larger than for other organic films of rodlike molecules, like pentacene.³²

Next, we would like to comment on some unusual features concerning the adsorption and desorption kinetics. The initial sticking coefficient of sufficiently large organic molecules is typically assumed to be 1 at and below room temperature.^{15,16} However, in this work, we could clearly demonstrate that the sticking coefficient increases with increasing coverage, which excludes an initial sticking coefficient of 1 for rubicene on SiO₂. Unfortunately, there exists little quantitative experimental and theoretical work in the literature on this subject, since all-atom molecular dynamics (MD) calculations of the adsorption dynamics of larger molecules are quite expensive. We are only aware of one theoretical work where the trapping dynamics of diindenoperylene (DIP) molecules on self-assembled monolayers (SAMs) have been studied, using MD simulations with MM3.³³ In that work, the authors showed that the sticking coefficient depends on several parameters, e.g., on the incidence energy, the angle of incidence, the molecule orientation and the packing density of the SAM. Actually, these phenomena are well-known for the adsorption of small molecules on rigid substrates, both for associative (e.g., CO) and dissociative adsorption (e.g., H₂), for which a wealth of experimental and theoretical data is available.^{34–36} Having these findings in mind, we can at least speculate as to the reason of the rather low initial sticking coefficient for rubicene on silicon dioxide of about 0.2 (0.25 on the C-covered surface, 0.17 on the clean surface). The fundamental question is whether sufficient energy can be transferred to the substrate for

accommodation within the interaction time. It was shown for the small molecule CO that the initial sticking coefficient on a variety of metal substrates decreases with increasing kinetic energy. Furthermore, the sticking coefficient decreases with decreasing adsorption energy.³⁷ This can be understood from simple classical arguments. The molecules have to transfer sufficient kinetic energy during the interaction with the surface to become trapped. The adsorption energy for the rubicene molecule ($C_{26}H_{14}$) on SiO_2 is 1.25 eV, which means that the binding energy per C atom is just about 50 meV. Thus, it is not implausible that the initial sticking coefficient is not 1. Another aspect is the orientation of the molecules in front of the surface during interaction with the surface. The influence of rotational energy on sticking has been shown by Batista et al.³⁸ for H_2O on ice and by Gardner et al.³⁹ for CO on ice substrates. It can be anticipated that the orientation effect will be even more pronounced for larger rigid molecules. Furthermore, the proper mass matching will be relevant for effective accommodation. This was shown, e.g., by McMaster et al.⁴⁰ for propane on platinum substrates. The authors explained the increase of the sticking coefficient with coverage by the better mass matching and a greater deformability of the adlayer. Finally, precursor mediated adsorption should be taken into account.⁴¹ In this scenario, the molecule is first trapped in a weakly bound state where it can still move along the surface until final accommodation, or desorb again during the residence time in the precursor state. The interaction with islands and other imperfections on the surface will increase the accommodation, which again will lead to an increase of the sticking coefficient with coverage.

Finally, some comments to the desorption behavior of rubicene from SiO_2 . From the desorption spectra, one cannot only determine the desorption energy but also the frequency factor for desorption, according to eq 2. In particular, the frequency factor contains information on the kinetics of desorption. For atoms and small molecules, the frequency factor can be correlated with the attempt frequency for desorption, which is in the order of 10^{13} s^{-1} . However, according to transition state theory,⁴² the pre-exponential factor contains the ratio of the partition functions of the molecules in the gaseous phase and the adsorbed phase. Due to the many rotational and vibrational degrees of freedom in the gas phase, the pre-exponential factor for large organic molecules is by orders of magnitudes larger than 10^{13} s^{-1} .¹³ In our particular case, we determine a frequency factor for the first-order desorption of the (sub)-monolayer phase of $\nu_1 \approx 10^{16} \text{ s}^{-1}$ and for the zero-order desorption from the multilayer phase $\nu_0 \approx 10^{18} \text{ s}^{-1}$. The lower frequency factor for the monolayer desorption might imply that the molecules in the (sub)-monolayer are more mobile than in the bulk phase prior to desorption.^{43,44}

5. SUMMARY AND CONCLUSIONS

The initial film formation of rubicene molecules on silicon dioxide exhibits a quite unusual behavior. First, a monolayer of flat-lying molecules is formed, followed by a second layer of flat-lying molecules. The desorption energy of these molecules is 1.25 eV. Deposition of further rubicene leads to a destabilization of this bilayer and to dewetting by the formation of 3D islands. The crystallographic structure of these islands is bulk-like, with the (001) plane being parallel to the substrate. This leads to an arrangement of upright standing but tilted molecules. The desorption energy for the molecules in the 3D

islands (heat of evaporation) is larger than that for the flat-lying molecules in the wetting layer, namely, 1.47 eV. This is the reason for the strong tendency of dewetting.

Dewetting of the bilayer can also be induced by exposing such a layer to air. This has been shown by thermal desorption spectroscopy and atomic force microscopy. Furthermore, for the island-like film under ambient conditions, Ostwald ripening was observed, leading to films composed of few, large crystalline islands. In the case of very thin films, most of the material in the small islands even disappeared by evaporation within several days at room temperature.

A further peculiarity of the adsorption system rubicene/ SiO_2 is related to the sticking coefficient. Contrary to common wisdom, the initial sticking coefficient is not 1, even at a substrate temperature of 220 K. We measured an initial sticking coefficient of only 0.2 ± 0.05 , depending on the substrate conditions. This low value can be related to the relatively weak interaction energy between the molecules and the substrate. However, other reasons connected with the adsorption dynamics can also play a role, e.g., orientational hindering, insufficient energy accommodation due to mass mismatch, or precursor mediated adsorption. This can be inferred from the fact that with increasing coverage the sticking coefficient increases, and probably approaches 1 for thicker films.

Adsorption and desorption of rubicene on SiO_2 is only weakly depending on the substrate chemical composition. Accumulation of carbon on the surface, due to some dissociation of rubicene during sample heating, does not significantly influence the shape of the desorption spectra nor the coverage dependence of the sticking coefficient. The reason for this is again the already weak interaction energy between rubicene and silicon dioxide, which is not further decreased by contaminations significantly.

■ ASSOCIATED CONTENT

S Supporting Information

Rubicene purification, crystal growth from solution, IR and optical spectroscopy, single crystal characterization with X-ray diffraction, thermal desorption from clean silicon dioxide, and determination of the desorption energy. This material is available free of charge via the Internet at <http://pubs.acs.org>.

■ AUTHOR INFORMATION

Corresponding Author

*E-mail: a.winkler@tugraz.at. Phone: ++43 316 873 8463.

Author Contributions

The manuscript was written through contributions of all authors. All authors have given approval to the final version of the manuscript.

Notes

The authors declare no competing financial interest.

■ ACKNOWLEDGMENTS

This work was financially supported by the Austrian Science Fund FWF, Proj. No. P 23530. We would like to acknowledge the group of Peter Wilhelm at the FELMI-ZFE for performing the FTIR microscopy measurements on the rubicene single crystals.

■ REFERENCES

- (1) Katz, H.-E.; Huang, J. Thin-Film Organic Electronic Devices. *Annu. Rev. Mater. Res.* **2009**, 39, 71–92.

- (2) Kranzelbinder, G.; Leising, G. Organic Solid State Lasers. *Rep. Prog. Phys.* **2000**, *63*, 729–762.
- (3) Kalyani, N. T.; Dhoble, S. J. Organic Light Emitting Diodes: Energy Saving Lightening Technology-A Review. *Renewable Sustainable Energy Rev.* **2012**, *16*, 2696–2723.
- (4) Mahns, B.; Roth, F.; König, A.; Grobosch, M.; Knupfer, M.; Hahn, T. *Phys. Rev. B* **2012**, *86*, 035209.
- (5) Bruker, APEX2 Software Suite (version 2.0-2); Bruker AXS Inc.: Madison, WI, 2005.
- (6) Sheldrick, G. M. A Short History of SHELX. *Acta Crystallogr., Sect. A* **2008**, *A64*, 112–122.
- (7) Sheldrick, G. M. SADABS, version 2.10; Siemens Area Detector Correction; Universität Göttingen, Germany, 2003.
- (8) Masel, R. I. *Principles of Adsorption and Reaction on Solid Surfaces*; John Wiley & Sons, Inc.: New York, 1996.
- (9) Frank, P.; Hlawacek, G.; Lengyel, O.; Satka, A.; Teichert, C.; Resel, R.; Winkler, A. Influence of Surface Temperature and Surface Modifications on the Initial Layer Growth of Para-Hexaphenyl on Mica(001). *Surf. Sci.* **2007**, *601*, 2152–2160.
- (10) <http://www.chemspider.com/Chemical-Structure.60779.html>
- (11) Desiraju, G. R.; Gavezzotti, A. Crystal Structures of Polynuclear Aromatic-Hydrocarbons-Classification, Rationalization and Prediction from Molecular-Structure. *Acta Crystallogr., Sect. B* **1989**, *45*, 473–482.
- (12) Cambridge Crystallographic Data Centre, 12 Union Road, Cambridge CB2 1EZ, U.K.; Supplementary publication no. CCDC 913540 (rubicene, 100 K) and CCDC 913541 (rubicene, 250 K).
- (13) Winkler, A. Thermal Desorption of Organic Molecules. *Springer Proc. Phys.* **2009**, *129*, 29–36.
- (14) Sauerbrey, G. Verwendung von Schwingquarzen zur Wägung Dünner Schichten und zur Mikrowägung. *Z. Phys.* **1959**, *155*, 206–222.
- (15) Müllegger, S.; Stranik, O.; Zojer, E.; Winkler, A. Adsorption, Initial Growth and Desorption Kinetics of p-Quaterphenyl on Polycrystalline Gold Surfaces. *Appl. Surf. Sci.* **2004**, *221*, 184–196.
- (16) Frank, P.; Djuric, T.; Koini, M.; Salzmann, I.; Rieger, R.; Müllen, K.; Resel, R.; Koch, N.; Winkler, A. Layer Growth, Thermal Stability, and Desorption Behavior of Hexaaza-triphenylene-hexacarbonitrile on Ag(111). *J. Phys. Chem. C* **2010**, *114*, 6650–6657.
- (17) Redhead, P. A. Thermal Desorption of Gases. *Vacuum* **1962**, *12*, 203–211.
- (18) Tumbek, L.; Gleichweit, C.; Zojer, K.; Winkler, A. Origin of the Bimodal Island Size Distribution in Ultrathin Films of Para-Hexaphenyl on Mica. *Phys. Rev. B* **2012**, *86*, 085402.
- (19) Müllegger, S.; Salzmann, I.; Resel, R.; Winkler, A. Epitaxial Growth of Quaterphenyl Thin Films on Gold(111). *Appl. Phys. Lett.* **2003**, *83*, 4536–4538.
- (20) Haber, T.; Müllegger, S.; Winkler, A.; Resel, R. Temperature-Induced Epitaxial Growth Modes of Para-Sexiphenyl on Au(111). *Phys. Rev. B* **2006**, *74*, 045419.
- (21) Andreev, A.; Matt, G.; Brabec, C. J.; Sitter, H.; Badt, D.; Seyringer, H.; Sariciftci, N. S. Highly Anisotropic Self-Assembled Structures of Para-Sexiphenyl Grown by Hot-Wall Epitaxy. *Adv. Mater.* **2000**, *12*, 629–633.
- (22) Balzer, F.; Rubahn, H.-G. Dipole-Assisted Self-Assembly of Light-Emitting p-nP Needles on Mica. *Appl. Phys. Lett.* **2001**, *79*, 3860–3862.
- (23) France, C. B.; Schroeder, P. G.; Forsythe, J. C.; Parkinson, B. A. Scanning Tunneling Microscopy Study of the Coverage-Dependent Structure of Pentacene on Au(111). *Langmuir* **2003**, *19*, 1274–1281.
- (24) Kilian, L.; Umbach, E.; Sokolowski, M. Molecular Beam Epitaxy of Organic Films Investigated by High Resolution Low Energy Diffraction (SPA-LEED): 3,4,9,10-Perylenetetracarboxylic –Dianhydride (PTCDA) on Ag(111). *Surf. Sci.* **2004**, *573*, 359–378.
- (25) Kury, P.; Roos, K. R.; Thien, D.; Möllenbeck, S.; Wall, D.; Horn-von Hoegen, M. Meyer zu Heringdorf, F.-J. Disorder-Mediated Ordering by Self-Interfactant Effect in Organic Thin Film Growth of Pentacene on Silicon. *Org. Electron.* **2008**, *9*, 461–465.
- (26) Ruiz, R.; Choudhary, D.; Nickel, B.; Toccoli, T.; Chang, K. C.; Mayer, A. C.; Clancy, P.; Blakely, J. M.; Headrick, R. L.; Iannotta, S.; et al. Pentacene Thin Film Growth. *Chem. Mater.* **2004**, *16*, 4497–4508.
- (27) Frank, P.; Koch, N.; Koini, M.; Rieger, R.; Müllen, K.; Resel, R.; Winkler, A. Layer Growth and Desorption Kinetics of a Discoid Acceptor on Au(111). *Chem. Phys. Lett.* **2009**, *473*, 321–325.
- (28) Bondi, A. Van der Waals Volumes+Radii. *J. Phys. Chem.* **1964**, *68*, 441–451.
- (29) Fleming, A. J.; Netzer, F. P.; Ramsey, M. G. Nucleation and 3-D Growth of Para-Sexiphenyl Nanostructures from an Oriented 2D Liquid Layer Investigated by Photoemission Electron Microscopy. *J. Phys.: Condens. Matter* **2009**, *21*, 445003.
- (30) Ratke, L.; Voorhees, P. W. *Growth and coarsening: Ostwald ripening in material processes*; Springer-Verlag: Berlin, Heidelberg, New York, 2002.
- (31) Balzer, F.; Schiek, M.; Wallmann, I.; Schäfer, A.; Lützen, A.; Rubahn, H.-G. Stability of Organic Nanowires. *Proc. SPIE, Nanophotonics Materials VIII* **2011**, *8094*, 809409.
- (32) Nickel, B.; Barabash, R.; Ruiz, R.; Koch, N.; Kahn, A.; Feldman, L. C.; Haglund, R. F.; Scoles, G. Dislocation Arrangements in Pentacene Thin Films. *Phys. Rev. B* **2004**, *70*, 125401.
- (33) Kaushik, A. P.; Clancy, P. Trapping Dynamics of Diindenoperylene (DIP) in Self-Assembled Monolayers Using Molecular Simulation. *Surf. Sci.* **2011**, *605*, 1185–1196.
- (34) Rendulic, K. D.; Winkler, A. Adsorption and Desorption Dynamics as Seen Through Molecular Beam Techniques. *Surf. Sci.* **1994**, *299–300*, 261–276.
- (35) Matsushima, T.; Shobatake, K. Surface Reaction Dynamics and Energy Partitioning. *J. Mol. Catal. A: Chem.* **2010**, *315*, 135–147.
- (36) Tully, J. C. Chemical Dynamics at Metal Surfaces. *Annu. Rev. Phys. Chem.* **2000**, *51*, 153–178.
- (37) Kneitz, S.; Gemeinhardt, J.; Steinrück, H.-P. A Molecular Beam Study of the Adsorption Dynamics of CO on Ru(0111), Cu(111) and a Pseudomorphic Cu Monolayer on Ru(0001). *Surf. Sci.* **1999**, *440*, 307–320.
- (38) Batista, E. R.; Ayotte, P.; Bilic, A.; Kay, B. D.; Jonsson, H. What Determines the Sticking Probability of Water Molecules on Ice? *Phys. Rev. Lett.* **2005**, *95*, 223201.
- (39) Gardner, D. O. N.; Al-Halabi, A.; Kroes, G.-J. The Effect of Initial Rotational Energy on the Adsorption of CO on the (0001) Face of Crystalline Ice-I-h at Hyperthermal Energies. *J. Phys. Chem. B* **2004**, *108*, 3540–3547.
- (40) McMaster, M. C.; Schroeder, S. L. M.; Madix, R. J. Molecular Propane Adsorption Dynamics on Pt(110)-(1 × 2). *Surf. Sci.* **1993**, *297*, 253–271.
- (41) Weaver, J. F.; Carlsson, A. F.; Madix, R. J. The Adsorption and Reaction of Low Molecular Weight Alkanes on Metallic Single Crystal Surfaces. *Surf. Sci. Rep.* **2003**, *50*, 107–199.
- (42) Zhdanov, V. P. Arrhenius Parameters for Rate-Processes on Solid Surfaces. *Surf. Sci. Rep.* **1991**, *12*, 183–242.
- (43) Paserba, K. R.; Gellman, A. J. Kinetics and Energetics of Oligomer Desorption from Surfaces. *Phys. Rev. Lett.* **2001**, *86*, 4338–4341.
- (44) Fichthorn, K. A.; Miron, R. A. Thermal Desorption of Large Molecules from Solid Surfaces. *Phys. Rev. Lett.* **2002**, *89*, 196103.